IGARSS 2023 - 2023 IEEE International Geoscience and Remote Sensing Symposium | 979-8-3503-2010-7/23/$31.00 ©2023 IEEE | DOI: 10.1109/IGARSS52108.2023.10281485

SPECTRAL UNMIXING AND THE POTENTIAL OF WORLDVIEW-3 SATELLITE DATA FOR PEGMATITE EXPLORATION

Douglas Santos[1], Ariane Mendes[1], Antônio Azzalini[1], Joana Cardoso-Fernandes[1,2], Alexandre Lima[1,2], Ana Cláudia Teodoro[1,2]

[1]Department of Geosciences, Environment and Spatial Planning, University of Porto, Porto, Portugal
[2]Institute of Earth Sciences (ICT), Porto, Portugal
*douglas.santos@fc.up.pt

ABSTRACT

Remote Sensing has been successfully applied in the identification of pegmatitic targets. However, the spatial resolution of open data satellites, which is often much larger than the outcrop size of the target mineral or rock, has been a recurrent challenge in this scientific field. This restricts remote sensing methods that are dependent on large outcrop sizes for successful identification. This work applied spectral unmixing approach on WorldView-3 satellite imagery, to evaluate the potential for high spatial resolution imagery on the Tysfjord Niobium-Yttrium-Fluorine (NYF) pegmatite field (Norway). The preliminary results of this research are encouraging and make a strong contribution to the scientific field of mineral exploration.

Index Terms — High-resolution imagery, NYF pegmatites, pegmatite exploration, Hourglass Spectral Wizard

1. INTRODUCTION

Several methods of remote sensing have been applied in pegmatite exploration. Pegmatites are an important source of critical resources, and their exploitation is important for Europe's economy. The methods applied ranged from distinct machine learning algorithms to target Lithium-Cesium-Tantalum (LCT) and Niobium-Yttrium-Fluorine (NYF) pegmatites [1], [2] to spectral unmixing approach. Spectral unmixing was recently applied to PRISMA hyperspectral data to map minerals of interest in Cornwall, UK [3].

However, the low spatial resolution of open multispectral data and hyperspectral satellites has, always, been a limiting factor to the potential of the results obtained. This research tests different classification methods based on spectral unmixing in high spatial resolution images from the WorldView-3 (WV3) satellite.

The main objectives of this study are to verify if (i) the higher spatial resolution can enhance the results obtained by previous classification methods [2], (ii) the Hourglass Spectral Wizard can select the target endmember correctly and (iii) if the classification methods are effective in identifying NYF pegmatites [2]. The methodology was applied through the Hourglass Spectral Wizard (HSW) Workflow. The HSW corresponds to a set of methods to select endmembers that are further used for image classification. The Mixture Tuned Matched Filtering [4], and the Spectral Angle Map Creator [5], were used to classify the whole image.

2. STUDY AREA

The study area has 100 km^2 and is located in the Tysfjord-Hamarøy pegmatite field in the Tysfjord district (Norway). This is an area with two important open pit mines (Jennyhaugen and Håkonhals). The majority of the pegmatite bodies are classified as NYF type and 157 minerals were identified in these rocks [6]. In a geological context, the area encompasses the granitic gneiss of the Trans-Scandinavian Igneous Belt [6]. In addition, the pegmatites are divided into two genetic groups, regarding their age, average body size and deformation degree. The first group is lenticular to cigar-shaped, with approximately 400 meters in size, while the second is younger and corresponds to smaller undeformed bodies [6]. For this work, the study area was divided into two parts - area 1(A1) and area 2 (A2) - to collect endmembers and to understand how the classification results perform concerning the target under study (pegmatite body).

3. DATA AND PRE-PROCESSING

The WV3 image, acquired on May 23, 2022, has been subdivided into four subsets. The P1 (SWIR bands) and P2 (VNIR bands) are in the east of the study area where the Jennyhaugem mine occurs. The P3 (SWIR bands) and P4 (VNIR bands) are in the west of the study area and encompass the Håkonhals mine. Together with the VNIR bands (P2, P4) is the panchromatic band with 0.5 m of ground-sampling distance (GSD), while the VNIR bands have 2 m GSD, and the SWIR bands have a spatial resolution of 3.7 m GSD.

In this work, tiled images were used, avoiding the need to make mosaics. An orthorectification was performed on the tiled images through the RPC Orthorectification Workflow (ENVI 5.6.3) [7]. Next, the *ATCOR Ground Reflectance* (PCI

Geomatica 2018) was applied to compute the surface reflectance and *haze removal* was performed in A2 images to minimize visible haze effects in this area. Even applying the haze removal, the haze present in area 2 impacted the visible bands, preventing correct image mosaic creation. Thus, it was decided to keep the separate images of area 1 and area 2.

4. IMAGE PROCESSING

The image processing is based on spectral unmixing approach to identify the most spectrally pure pixels. This method, applied through the HSW workflow, allows us to select and extract the target endmembers for classification. The step-by-step image processing is shown in Figure 1.

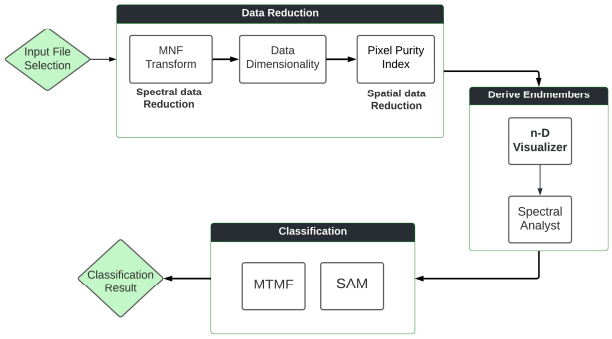

Figure 1. Step by Step of Spectral Hourglass Wizard Workflow.

Minimum Noise Fraction (MNF) was used to equalize and segregate the noise from the data, to spectrally reduce the data and computational requirements for subsequent processing [8]. While the noise is concentrated in the last bands, the lower numbered bands (coherent images) concentrate the high information content [9]. An MNF transform was performed for all 16 bands for each study area.

Data Dimensionality allows the analyst to determine spatial coherence more accurately. The Data Dimensionality panel indicates coherence bands and allows the user to modify the threshold level to separate the signal from noise [10]. All bands above the threshold are considered noise and were not used in the next steps. Four bands were selected with a threshold of 0.78 for A1. For A2 three bands were selected with a threshold level of 0.96.

Pixel Purity Index (PPI) finds the most spectrally pure pixels by applying a spectral redundancy analysis on the data, allowing the selection of the target minerals endmembers in the next steps [8], [11]. The PPI was performed considering 10,000 iterations and a threshold of 5.0 for both study areas.

The n-D Visualizer computed a scatter plot through the endmembers derived from the PPI. The n-dimensional visualizer (n-D Visualizer) represents the spectra as points in a data cloud where *n* represents the number of bands [10]. It is known that the most spectrally unique material in the image resides at the corners of the data cloud. Therefore, is possible to select and extract the endmembers that are evaluated and exported through the spectral analyst tool [12]. In this stage, the spectra were analyzed to detect patterns and distinguish possible mineral spectra from the other elements. Although a more detailed distinction is made after the classification results analyses, four endmembers were selected for each study area. *Mixture Tuned Matched Filtering (MTMF)* performs Matched Filtering (MF) to find the abundances of a defined endmember through partial unmixing [4]. This method maximizes the response of the defined endmember and suppresses the response of the composite unknown background [4], [9]. The MTMF results in a set of rule images corresponding to both the MF score and the infeasibility score for each pixel compared to each endmember [4]. Using the endmembers retrieved from n-D Visualizer, MTMF resulted in four MF bands for each study area.

Spectral Angle Map (SAM) Creator algorithm uses an n-D angle to match the image pixels to reference spectra, comparing the angle between the endmember spectrum vector and each pixel vector in an n-D space [11]. The classification results helped to analyze the distribution of the elements under study forming multiple clusters of possible target pixels [5]. Same as MTMF, the SAM classification results in four classes for each study area. The maximum angle chosen for classification was 0.10.

5. PRELIMINARY RESULTS AND DISCUSSION

After extracting, exporting, and analyzing the data using the spectral analyst tool, we noticed that concerning A1 (Figure 2 a) the n-D class 1 has very low reflectance compared to the other spectra. After the classification, it was clear that this endmember corresponds to water bodies.

The n-D class 2 has absorption features (in bands 11, 12, 14, and 16) and reflectance peaks (in bands 10, 13, and 15) more expressive in the SWIR region. This is a characteristic pattern of minerals and rocks, which indicates that this endmember is a possible target. This analysis was confirmed during the classification process, where it is noticeable that this endmember was used to correctly classify areas of known pegmatite bodies.

The n-D class 3 has significant absorption in the VNIR region (bands 3 and 6) and in the SWIR (bands 8 and 11). After classification, this endmember corresponds to snow.

The n-D class 4 has a reflectance peak that starts in the Red Edge band (band 6) and another peak in the SWIR 1 (band 8) that remains stable until the SWIR 2 (band 10). This endmember corresponds to areas classified as agricultural fields and native vegetation [13].

Regarding A2, (Figure 2 c), n-D class 1 has very low reflectance with values near 0. In the classification, this endmember was classified as water.

The n-D class 2 and n-D class 3 have very similar reflectance to each other and are also very similar to n-D class 4 of A1. In these two endmembers it is possible to notice two absorptions in the VNIR region (band 3 and 5) that can indicate the presence of chlorophyll [14]. This double absorption together with reflectance peaks in the NIR region

(band 7) and early SWIR (band 9) may represent the NIR plateau. This plateau is characteristic of vegetation which was corroborated in the classification results.

Finally, n-D class 4 presents very expressive absorptions in the SWIR region (bands 11, 12, 14, and 16), and similar to n-D class 2 of A1 was also confirmed by correctly mapping the target pegmatites in the classification.

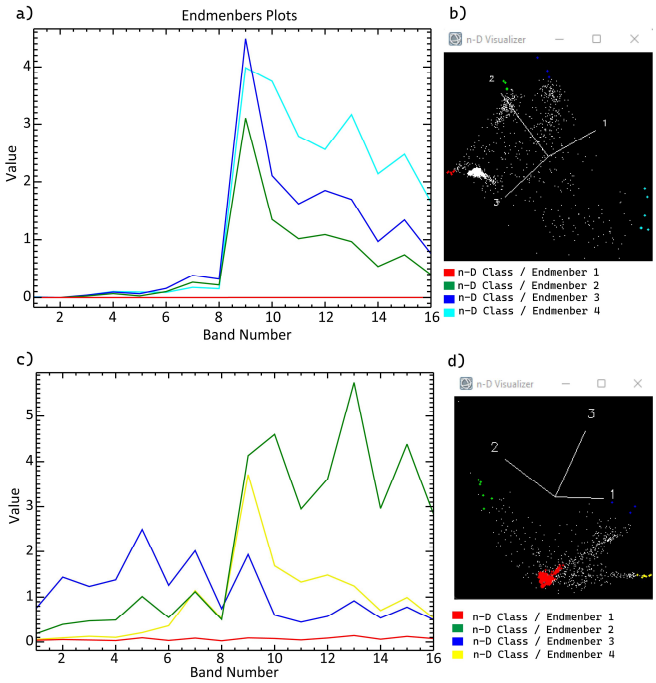

Figure 2. Endmembers extracted through the n-D Visualizer panel. a) Spectra derived from the data cloud for Area 2. b) multi-dimensional scatter plot indicating, in clusters, where Area 2 endmembers were selected. c) Spectra derived from the data cloud for Area 1. d) multi-dimensional scatter plot indicating, in clusters, where Area 1 endmembers were selected.

In summary, the endmembers corresponding to the target are endmembers 2 (A1) and endmember 4 (A2). The spectral similarity of n-D class 2 and 3 (A2) suggests that the angle of the scatter plot of Figure 2 b indicates two ends. These ends look distinct but represent very similar endmembers.

Comparing these results with the Corine Land Cover (CLC)[13] map shows that endmember 4 (A1) corresponds to agricultural fields and native vegetation areas. While endmembers 2 and 3 (A2) encompass agricultural fields, native vegetation, and broad-leaved forest zones. This is worth future investigation, as it may indicate that closely spaced corner points are variants of the same element. We should focus our selection on endmembers that lie on the corners of the scatter plot rather than on their extreme ends.

The classification results (Figure 3) were treated in a GIS environment to highlight pegmatite pixels from the background. To determine this threshold, the pixel values of the Hakonhals and Jennyhaugem mines were analyzed for each classification method. Analyzing the MTMF results it is evident that the MF bands that correspond to pegmatites are MF bands 2 (A1) and 4 (A2). For these results, the pixels of the mines have a value varying between 70 and 255.

A reclassification was made where the pixels with a higher value (255) were represented in red color. Those with an intermediate value (200 to 254) in light red color, and those with a lower value (70 to 199) in orange color.

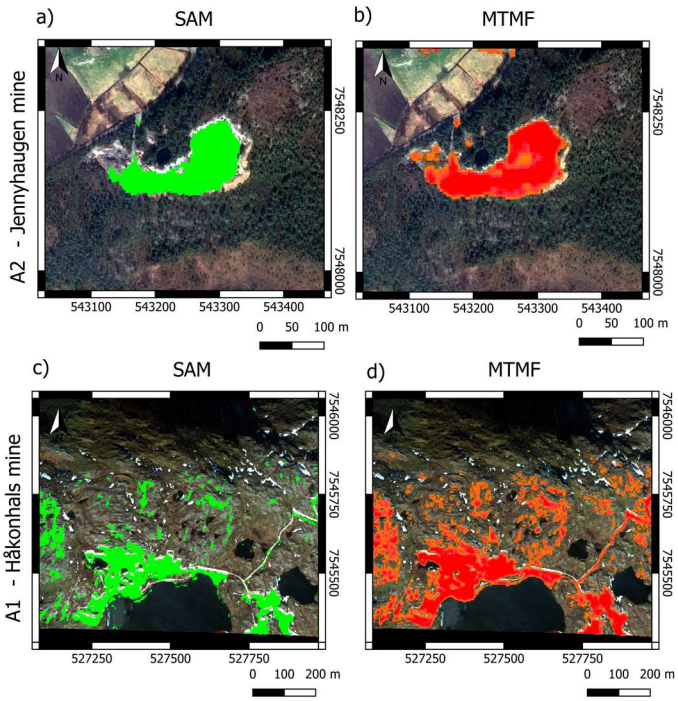

Figure 3. Classification results. a) SAM classification results for Jennyhaugen mine. b) MTMF classification results for Jennyhaugen mine. c) SAM classification results for Håkonhals. d) MTMF classification results for Håkonhals mine.

The pixels with a value of less than 70 were disregarded. This reclassification allowed the formation of clusters that highlight the pixels of greatest interest and help to analyze the result of the MTMF classification. As can be seen in Figure 3 b and c, the pixels with higher values occupy most of the mines' exposed rock. This behavior forms clusters that can be observed in other known pegmatite points.

The false positives are mostly concentrated on roads and coastal areas. However, the greater part of the false positives is represented by pixels of low and intermediate value. This indicates that focusing the analysis on the higher values is the most accurate method for target identification. These higher-valued pixels can also be pre-selected in the final steps of the HSW workflow, which allows the user to adjust the values of the MF bands via histogram analysis.

The SAM method results in a single image with classes that correspond to the number of endmembers used in the classification. Therefore, for both study areas, we have an image with four classes. Same as the MTMF, the classes that correspond to the target are class 2 (A1) and class 4 (A2). However, in opposition to the MTMF, the pixels of each class have a single value that corresponds to the class to which they belong. This limits the analysis and fuzzification of results, which leads to more false positives than the MTMF.

Comparing the results with the classification of previous work with Sentinel 2 images [2], it is noticeable that the classification from the WV3 images is much more refined and has fewer false positives due to better discrimination between pegmatites and granite. Of the 17 known pegmatite points (including the two open-pit mines), nine points were correctly identified by both methods (53% of pegmatites spots correctly identified). However, the points that were not identified correspond to old mines whose excavations appear with shadows in the image and do not have areas exposed in the open pit. This hinders their correct identification through the classification methods.

In summary, the method was successful in selecting the endmembers that correspond to our target. This, coupled with the high resolution of the WV3 images, allowed to perform an effective classification to identify known pegmatites.

6. CONCLUSION

The high spatial resolution of the WV3 images resulted in a classification with fewer false positives with granite, which has always been a difficulty in previous classifications using lower GSD images. The selection of endmembers in the data is the key to the success of the spectral unmixing technique. Through the data cloud, it was possible to select the target endmenber successfully. The time invested in this step will determine the quality of the classification results. The results show that the combination of a spectral unmixing method and a high-resolution image is a powerful tool for NYF pegmatite exploration. Although the MTMF obtained better results by allowing a more interactive analysis by the user, the results of the SAM method can also be refined. The proposed method can be applied to other areas to identify other pegmatite types. The results obtained are encouraging and allowed to understand the potential of WV3 for the pegmatite exploration field. These results together with other data, such as Light Detection And Ranging (LiDAR) data, will be used to identify and map new points of interest for pegmatite exploration in future works.

7. ACKNOWLEDGEMENTS

This study is funded by European Commission's Horizon 2020 innovation program under grant agreement no. 869274, project GREENPEG. The work is co-funded by national funds by FCT–Fundação para a Ciência e a Tecnologia, I.P., in the framework of the ICT project with the references UIDB/04683/2020 and UIDP/04683/2020.

8. REFERENCES

[1] J. Cardoso-Fernandes, A. C. Teodoro, A. Lima, and E. Roda-Robles, "Semi-Automatization of Support Vector Machines to Map Lithium (Li) Bearing Pegmatites," *Remote Sens.*, vol. 12, no. 14, 2020, doi: 10.3390/rs12142319.

[2] D. Santos, J. Cardoso-Fernandes, A. Lima, A. Müller, M. Brönner, and A. C. Teodoro, "Spectral Analysis to Improve Inputs to Random Forest and Other Boosted Ensemble Tree-Based Algorithms for Detecting NYF Pegmatites in Tysfjord, Norway," *Remote Sens.*, vol. 14, no. 15, p. 3532, 2022, doi: 10.3390/rs14153532.

[3] D. Santos, A. Lima, and A. C. Teodoro, "The potential of spectral unmixing method applied to PRISMA hyperspectral images in the evaluation for prospecting purposes," vol. 1226811, no. October, 2022, doi: 10.1117/12.2636034.

[4] L3Harris. (2020, 01 November 2022). *Mixture Tuned Matched Filtering*. Available: https://www.l3harrisgeospatial.com/docs/mtmf.html.

[5] A. Panda and D. Pradhan, "Hyperspectral image processing for target detection using Spectral Angle Mapping," *2015 Int. Conf. Ind. Instrum. Control. ICIC 2015*, no. Icic, pp. 1098–1103, 2015, doi: 10.1109/IIC.2015.7150911.

[6] A. Müller *et al.*, "Two-stage regional rare-element pegmatite formation at Tysfjord, Norway: implications for the timing of late Svecofennian and late Caledonian high-temperature events," *Int. J. Earth Sci.*, vol. 111, pp. 987–1007, 2022, doi: 10.1007/s00531-022-02166-5.

[7] B. Pradhan, A. A. Ahmed, S. Chakraborty, A. Alamri, and C.-W. Lee, "Orthorectification of WorldView-3 Satellite Image Using Airborne Laser Scanning Data," *J. Sensors*, vol. 2021, 2021, doi: 10.1155/2021/5273549.

[8] P. S. Mujabar and S. Dajkumar, "Mapping of bauxite mineral deposits in the northern region of Saudi Arabia by using Advanced Spaceborne Thermal Emission and Reflection Radiometer satellite data," *Geo-Spatial Inf. Sci.*, vol. 22, no. 1, pp. 35–44, 2019, doi: 10.1080/10095020.2018.1530857.

[9] R. J. Ellis and P. W. Scott, "Evaluation of hyperspectral remote sensing as a means of environmental monitoring in the St. Austell China clay (kaolin) region, Cornwall, UK," *Remote Sens. Environ.*, vol. 93, no. 1, pp. 118–130, 2004, doi: https://doi.org/10.1016/j.rse.2004.07.004.

[10] J. D. Wolfe and S. R. Black, "Hyperspectral Analytics in ENVI," 2018, [Online]. Available: www.harrisgeospatial.com

[11] F. A. Kruse *et al.*, "The spectral image processing system (SIPS)—interactive visualization and analysis of imaging spectrometer data," *Remote Sens. Environ.*, vol. 44, no. 2, pp. 145–163, 1993, doi: https://doi.org/10.1016/0034-4257(93)90013-N.

[12] B. Hu, Y. Xu, B. Wan, X. Wu, and G. Yi, "Hydrothermally altered mineral mapping using synthetic application of Sentinel-2A MSI, ASTER and Hyperion data in the Duolong area, Tibetan Plateau, China," *Ore Geol. Rev.*, vol. 101, no. July, pp. 384–397, 2018, doi: 10.1016/j.oregeorev.2018.07.017.

[13] European Union;, "Copernicus Land Monitoring Service 2018, European Environment Agency (EEA)"

[14] A. R. Huete, *Remote Sensing for Environmental Monitoring*. Elsevier, Inc., 2004. doi: 10.1016/B978-012064477-3/50013-8.